International Journal of Cast Metals Research

ISSN: 1364-0461 (Print) 1743-1336 (Online) Journal homepage: http://www.tandfonline.com/loi/ycmr20

Solidifying pressure and microstructure of AlSi10Cu3 in die sleeve in high pressure die casting

X. P. Hu, G. Q. Zhao & W. M. Wang

To cite this article: X. P. Hu, G. Q. Zhao & W. M. Wang (2010) Solidifying pressure and microstructure of AlSi10Cu3 in die sleeve in high pressure die casting, International Journal of Cast Metals Research, 23:5, 289-295, DOI: 10.1179/136404610X12693537270136

To link to this article: http://dx.doi.org/10.1179/136404610X12693537270136

Published online: 18 Jul 2013.

Solidifying pressure and microstructure of AlSi10Cu3 in die sleeve in high pressure die casting

X. P. Hu*[1], G. Q. Zhao[2] and W. M. Wang[2]

The microstructure and microhardness of AlSi10Cu3 solidified in a die sleeve were studied, and the differential equation of local solidifying pressure was deduced in horizontal cold chamber high pressure die casting. The local solidifying pressure changed, and in the last stage of solidification, porosity and pores were present because of the decreasing pressure. Microhardness relative to microstructure varied with locations, the minimum value being observed at 40% of the radius from the biscuit centre. Temperature distribution analysis carried out with ANSYS showed the solidified thickness to be proportional to $t^{1/2}$ in the initial 7 s of solidification; in the final stage of solidification, the solidified layer thickened faster and its thickness was proportional to $t^{8{\cdot}4631}$. Microsegregation of AlSi10Cu3 was observed in the die sleeve and Si precipitated in fine granules, dendrites and coarse granules in morphology from exterior to centre.

Keywords: High pressure die casting, Solidifying pressure, Microstructure, AlSi10Cu3, Die sleeve

Introduction

Al–Si alloy is the most widely used die casting alloy all over the world, and with the tendency of light metal substitution for steel to reduce vehicle weight and improve fuel economy in automobile industry,[1,2] near eutectic Al–Si alloy would become more and more important. There are two macrostages when liquid metal becomes castings in die casting. One is die filling and the other is solidification. In die filling, the liquid metal passes through the die sleeve and gating system, enters in and is full of the cavity. In solidification, the liquid metal solidifies under high pressure and replicates the cavity. The alloy in die sleeve played an important role in die casting and much attention was paid in last 10 years. For example,

(i) in order to improve die casting efficiency, the thermal distortion and thermal fatigue in shot sleeves were studied in the Ohio State University.[3–5] They pointed out that the improved sleeves had a major impact on dimensional stability, reproducibility and quality of the product, and they studied these problems by means of finite element analysis and experiments on different material compositions and types of die sleeves. However, the pressure effects on die sleeve and the product were not mentioned

(ii) in order to enhance the die castings' properties such as porosity and strength, the air entrapment and the slow shot were studied.[6–8] They developed coupled fluid flow and solidification model to study the liquid metal in die sleeve, and the liquid surface waves and pore distribution were emphasised. They explored the effects of the shot velocity, especially the slow velocity on air entrapment, but the pressure effects on phase structure of solidified liquid were not mentioned.

However, die sleeve is simple in structure and has cylinder-like shape, so some detail studies could be extended easier and much more comprehensive. The liquid alloy flowing and solidifying in die sleeve may affect the melt fluidity, cavity fill, microstructure and mechanical properties of final castings.[5,9–11] So, the authors chose the alloy in die sleeve to study the solidifying pressure in die casting. The objectives of this research are to investigate the relationships of microstructure and solidifying pressure, to examine the local solidifying pressure in die sleeve, and to provide criterion on improving strength in castings in foundry state.

Experimental material and procedure

Because the most widely used Al–Si alloys are near eutectic point, the authors chose AlSi10Cu3 to fulfil the experiment. The chemical composition of Al–Si alloy in holding furnace before die casting machine was shown in Table 1, and they were measured by spectral analyser in experimental factory.

[1]School of Mechanical Engineering, Shandong Institute of Light Industry, 2 Daxue Road, Jinan 250353, China
[2]School of Material Science and Engineering, Shandong University, 73 Jingshi Road, Jinan 250061, China

*Corresponding author, email zcqhuxx@sdu.edu.cn

Received 2 February 2008; accepted 9 February 2010
DOI 10.1179/136404610X12693537270136

A TOYO BD-650-V_2C die casting machine and a die named K90 right transmission case were used in the present research. Some parameters of die casting machine and die casting processes were shown in Table 2.

The microstructure were observed and photographed under Quanta 200E SEM. In order to prevent the pollution of sample making environment and to observe expediently, the observing samples were washed by ultrasonic washer and then a thin Au layer were plated under vacuum. The etching solution was 5%NaOH liquor solution.

The hardness was measured by HXD-1000TMC microhardness tester with picture analysis system, and the temperature distributions were analysed by ANSYS software and the pressure distribution were calculated by the arithmetic the authors developed below.

The samples were cut from biscuit according to the illustration in Fig. 1.

Experiments results

The SEM images of the sections observed were shown in Fig. 2. The microstructures of the solidified AlSi10Cu3 were shown in Fig. 2 in 0·95*R*, 0·7*R*, 0·4*R* and 0·1*R* from the biscuit centre respectively, and the sections where to be observed were also seen in Fig. 1*d*. The morphology of solidified alloy was in fine granules, dendrites, finer spacing dendrites with flakes, and coarse granules respectively.

The microhardnesses of sample in corresponding locations were shown in Fig. 3. The points 1–4 showed the mean microhardnesses of the solidified AlSi10Cu3 measured in sections which was 0·95*R*, 0·7*R*, 0·4*R* and 0·1*R* from the biscuit centre respectively. It showed that the maximum measured hardness was not in the near surface of biscuit, and the minimum measured hardness appeared at the 0·4R from the biscuit center.

Expatiations of Al–Si solidifying pressure

Differential equation of solidifying pressure

In full automatic die casting, the liquid alloy are poured into die sleeve through the pouring hole with ladling system mounted on die casting machine, and the temperature of AlSi10Cu3 in holding furnace is always 650–680°C. Unlike pure metal, AlSi10Cu3 does not solidify at a determinate temperature; it begins to solidify at 595°C and ends at 550°C according to the phase diagram. After pouring, the plunge tip was pull forward by shot piston in die cast machine. There were usually three stages of the plunge moving, slow velocity, fast velocity and accumulator pressure enlarger moving. When the liquid alloy was full of the cavity, the plunge tip contacted the alloy tightly. In solidification, the plunger tip moved forwards to compensate the volume of alloy which decreased with the shrinkage caused by temperature dropping and liquid–solid state transferring, and the pressure behind the shot piston was kept constant. The ingate zone of gating system solidified firstly because of thin thickness, and then, the liquid alloy in die sleeve could not feed the cavity anymore and they solidified under the mechanical pressure caused by plunge tip.

Table 1 Chemical composition of AlSi10Cu3 used, wt-%

Al	Si	Mn	Sn	Fe	Mg	Ni	Cu	Zn
Bal.	10·99	0·1842	0·0828	0·7426	0·1372	0·0330	2·433	0·7075

Table 2 Some machine parameters and die casting parameters

Clamping force, kN	6370 (max.)
Die thickness, $\times 10^{-3}$ m	350–900
Injecting force, kN	540 (max.)
Cycling time, s	85
Die stroke, $\times 10^{-3}$ m	660
Injecting temperature, °C	630
Diameter of biscuit, $\times 10^{-3}$ m	90
High speed, m s^{-1}	1·8
Low speed, m s^{-1}	0·3
High speed interval, $\times 10^{-3}$ m	110
Pouring weight, kg	2·6
Biscuit height, $\times 10^{-3}$ m	30

There were water passages in divider cone and plunge tip, and the alloy between them was we discussed in this paper. There were also water cooling linings in sleeve. So, a calculating model with coordinate system was concluded in Fig. 4 in the present horizontal cold chamber high pressure die casting. Before deduction, the authors supposed that:

(i) the alloys are all in liquid state and the temperatures distribute evenly
(ii) there existed centrelines in biscuit and only a square of biscuit is discussed in temperature analysis and microstructure observing because of symmetries
(iii) only alloys in sleeve were discussed.

After die filling, it is obviously that

$$P_0^{\mathrm{L}} = \frac{F}{\pi R^2} \tag{1}$$

$$V_0^{\mathrm{L}} = \pi R^2 H \tag{2}$$

where P_0^{L} and V_0^{L} are the initial pressure (Pa) and the volume (m^3) of liquid Al–Si alloy respectively, F is the injecting force (N), R is the radius of plunge tip (or biscuit) (m) and H is height of biscuit in liquid state (m).

After t seconds, some of the liquid solidified, and the solid/liquid interface would be in the position of x and y along the X and Y axes respectively, and

$$V_{\mathrm{t}}^{\mathrm{L}} = \pi(R-y)^2(H-x) \tag{3}$$

$$P_{\mathrm{t}}^{\mathrm{L}} = \frac{F-\pi\sigma_{\mathrm{C}}\left(R^2-y^2\right)}{\pi y^2} \tag{4}$$

where $P_{\mathrm{t}}^{\mathrm{L}}$ and $V_{\mathrm{t}}^{\mathrm{L}}$ are the pressure (Pa) and the volume (m^3) of liquid Al–Si alloy respectively in time t, σ_{c} is compressive strength of Al–Si alloy at high pressure and temperature (Pa), $(R-y)$ is solidified thickness (m). When the solidifying velocity is v (m s^{-1}), then at time $t+\mathrm{d}t$

$$V_{\mathrm{t+dt}}^{\mathrm{L}} = \pi\left(R-y-v_{\mathrm{y}}\mathrm{d}t\right)^2\left(H-x-v_{\mathrm{x}}\mathrm{d}t\right) \tag{5}$$

$$P_{\mathrm{t+dt}}^{\mathrm{L}} = \frac{F-\pi\sigma_{\mathrm{C}}\left[R^2-\left(y-v_{\mathrm{y}}\mathrm{d}t\right)^2\right]}{\pi\left(y-v_{\mathrm{y}}\mathrm{d}t\right)^2} \tag{6}$$

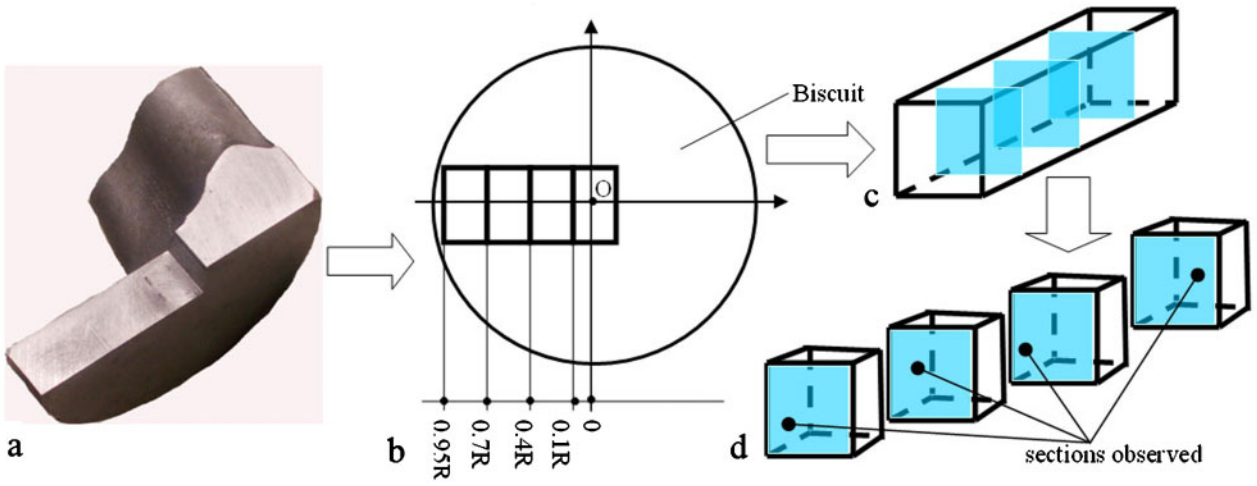

a biscuit after cut; *b* position to be cut; *c* stick cut away from biscuit; *d* sections observed

1 Illustration of samples extracted from biscuit

where $P_{t+dt}{}^{L}$ and $V_{t+dt}{}^{L}$ are the pressure (Pa) and the volume (m^3) of liquid Al–Si alloy respectively in time $t+dt$, and v_x and v_y are solidifying velocities (m s^{-1}) in x and y directions respectively.

According to the theory of solidification on the base of energy conservation, the solidifying height of casting and the solidifying time obey the equation below

$$t=\alpha_x(H-x)^2+\beta_x(H-x)=\alpha_y(R-y)^2+\beta_y(R-y) \quad (7)$$

where α_x, α_y, β_x and β_y are constants defined by the liquid alloy properties, mould material properties and the heat transferring conditions.

Considering the similar heat transferring conditions of X and Y directions, the solidifying velocities of the two directions may have relations below

$$v_x \propto v_y \quad (8)$$

The plunge tip moves a Δ gap within duration dt, which is mainly caused by liquid–solid phase transfer shrinkage and the volume shrinkage of solid and liquid. In order to be more convenient for discussion, Δ is neglected here because it is very small in value.

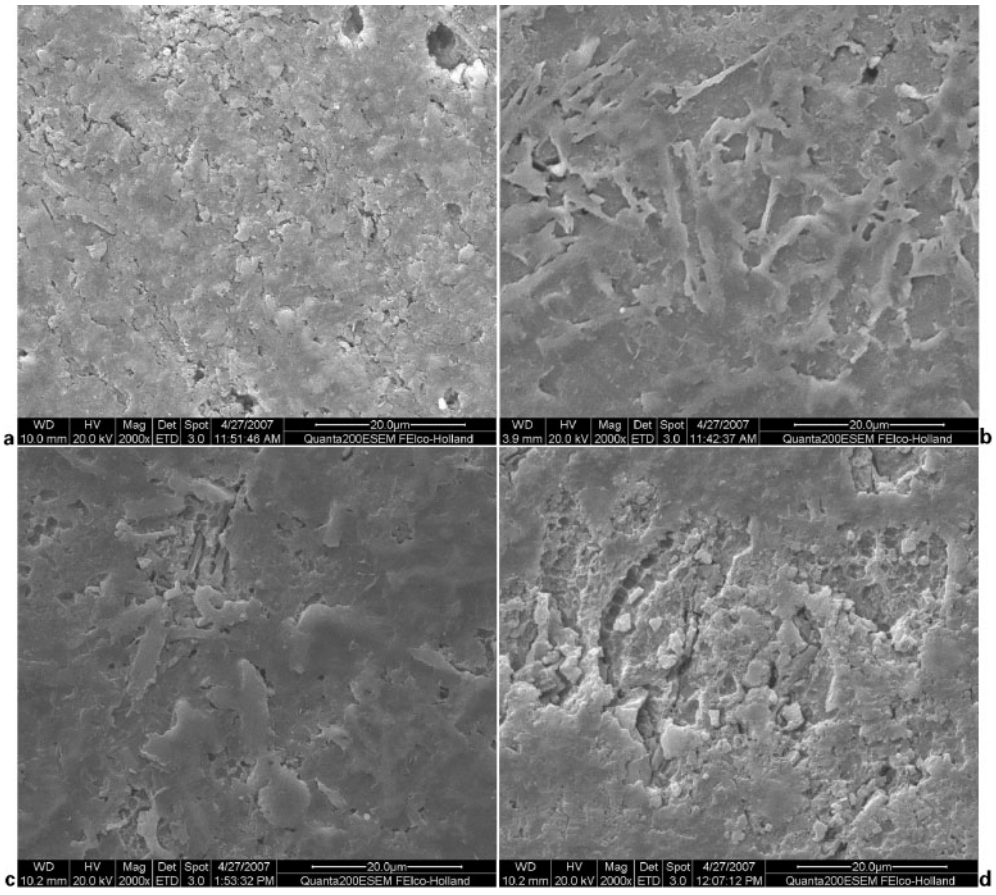

a 0·95*R* from biscuit centre; *b* 0·7*R* from biscuit centre; *c* 0·4*R* from biscuit centre; *d* 0·1*R* from biscuit centre

2 Microstructures of samples in different positions under SEM

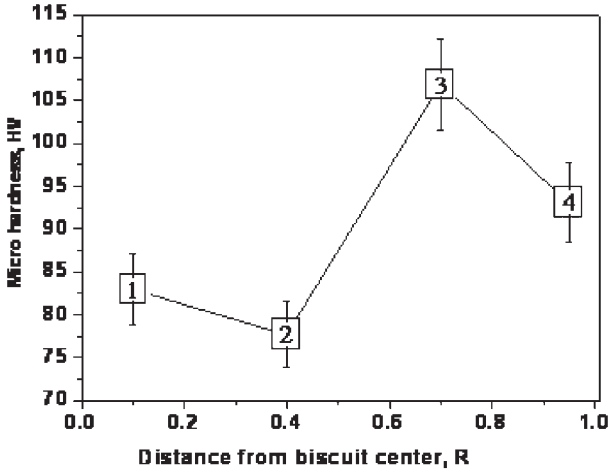

3 Microhardness measured

From equations (3)–(8), it can be inferred that

$$\frac{\mathrm{d}V^{\mathrm{L}}}{\mathrm{d}t} = -C_2(R-y)^2 v_{\mathrm{y}} \tag{9}$$

$$\frac{\mathrm{d}P^{\mathrm{L}}}{\mathrm{d}t} = \frac{2F-2\pi\sigma_{\mathrm{C}}R^2}{\pi y^3} v_{\mathrm{y}} \tag{10}$$

Equation (9) shows that the volume of liquid decreased with the solidifying time, and the decreasing velocity is proportional to the solidifying velocity and determined by the liquid alloy properties, mould material properties and the heat transferring conditions.

Equation (10) shows that the local solidifying pressure is determined by two factors, the injecting force and the compressive strength of solidified alloy.

When at high temperature, the compressive strength is very low, and the solidified layer would be in mushy state. Under three-direction compression, the solidified layer would have good plasticity and the strength would become higher than that in ordinary pressure. With decreasing temperature, the strength of solidified layer became higher and higher. When it is strong enough to endure injecting force of the plunge tip, the pressure in liquid metal began to decrease. If the shrinkage induced by temperature dropping is smaller than the shrinkage induced by phase changing, there would be porosity in biscuit.

At the beginning of solidification, the shrinkage of the liquid–solid transferring was bigger than the shrinkage induced by temperature dropping, but the injecting force acted on the plunge tip, and pushed the alloy to compensate the total shrinkage, and the pressure in liquid alloy could not decrease. Only at the last stage of solidification, the solidified layer was strong enough; the injecting force could not push the alloy forward to compensate liquid–solid transferring shrinkage, and the pressure in liquid alloy decreases. The pressure in retained liquid was determined by the shrinkage of solid and liquid alloys.

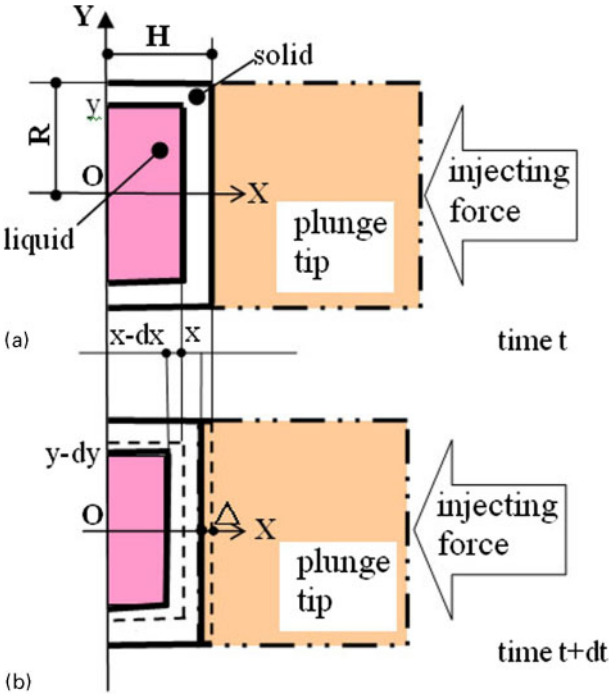

a* at time *t*; *b* at time *t*+d*t

4 Pressure calculating model in horizontal cold chamber high pressure die casting

Temperature distribution

In order to find the liquid pressure while solidifying, the temperature distribution and σ_{C} in die sleeve should be confirmed first. Considering the temperature and pressure, quoting some selected parameters in Zhang *et al.*'s[12] and Griffiths *et al.*'s[13] work, the parameters we used were shown in Table 3.

The ANSYS software was used and the latent heat was treated as enthalpy which the alloy included. The enthalpy applying examples in solidification simulation can also be seen in Postek *et al.*'s work.[14] The detail arithmetic based on the law of energy conservation was ignored here; the analysis results of temperature histories in different spots and temperature graphs at different solidifying times of solidifying Al–Si alloy in sleeve were shown in Figs. 5 and Fig. 6 respectively.

When the spot temperature was below 550°C, the liquid here was thought to be turned into solid totally.

Table 3 Parameters used in analysis with ANSYS*

AlSi10Cu3	Thermal conductivity, W m^{-1} K^{-1}	145
	Density, kg m^{-3}	$2{\cdot}646\times10^{3}$–$2{\cdot}8\times10^{-1}T$
	Initial temperature, °C	630
	Enthalpy, J m^{-3}	0 (0)
		$1{\cdot}343\times10^{9}$ (550°C, T_{S})
		$2{\cdot}422\times10^{9}$ (595°C, T_{L})
		$2{\cdot}679\times10^{9}$ (700°C)
Die sleeve	Temperature, °C	300
	Diameter, $\times10^{-3}$ m	90
Heat transfer coefficient, W m^{-2} °C^{-1}		20 000

*T_{S}: solid line in phase diagram; T_{L}: liquid line in phase diagram.

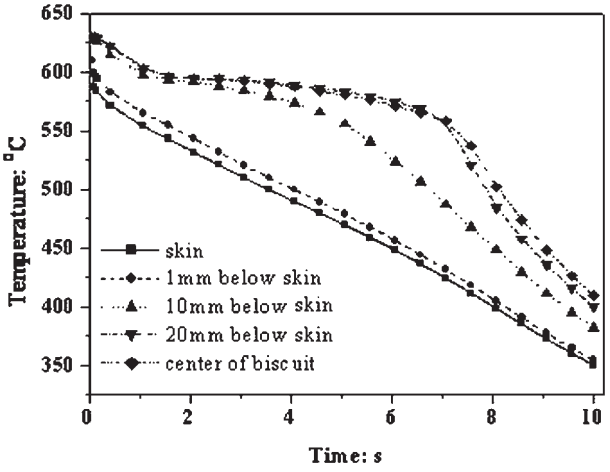

5 Temperature histories of solidifying Al–Si alloy in sleeve

Reviewing the temperature distribution of the cross-section, the thickness of solidified layer could be determined. The solidified thicknesses of 630°C AlSi10Cu3 in sleeve changed with time were shown in Fig. 7.

Local solidifying pressures

When solidifying, the temperature and pressure of liquid alloy changed with time. When the temperature of Al–Si alloy dropped near to solid line in Al–Si phase diagram, the solidified layer would have strength. However, it was not strong enough to endure the injecting force and may be crashed because of shear and compressive stress caused by plunge tip. Only after the value of average strength was larger than F/A (F is the injecting force in N, A is the area of biscuit cross section in m^2), the solidified layer could exist firmly, and according to equation (4), the local pressures began to decrease. The local solidifying pressure in the last stage of solidification in the present case was shown in Fig. 8. The average strengths of alloy under high pressure at high temperature were 85 MPa (505°C, 80 MPa), 86 MPa (500°C, 80 MPa) and 88 MPa (450°C, 80 MPa), and they were 310 MPa under 25°C and 0·1 MPa (1 atm).

In fact, in the last stage of solidification, the alloy possesses large plasticity because it is compressed from three directions, and there existed pressure loss because

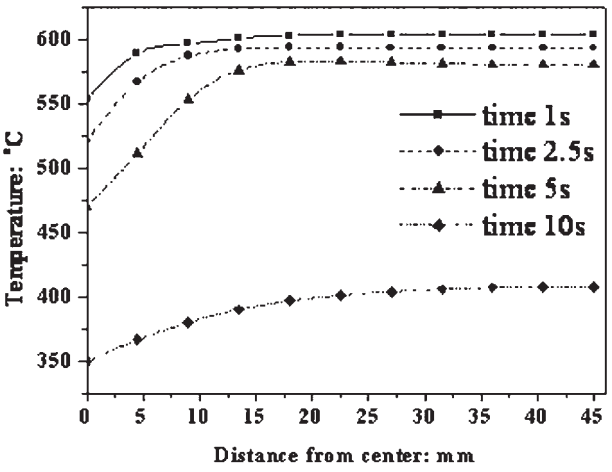

6 Temperature graphs of Al–Si alloy in sleeve at different solidifying times

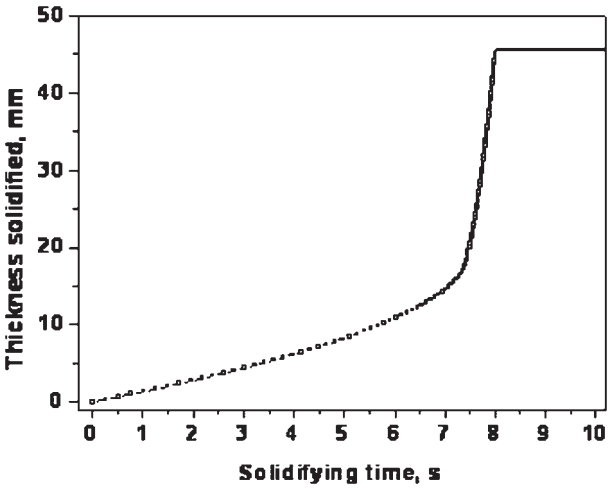

7 Solidified thickness graph in sleeve

of frictions. The pressure loss was related to alloy temperature, the distance from plunge tip, the injecting pressure, etc. The larger injecting pressure, the less pressure loss would be.[15]

Discussion

In the near eutectic Al–Si alloy, under non-equilibrium solidification, needle-like Si precipitated with the Al eutectic. The melting entropy of Al is about one-third that of Si, which is reflected in the fact that Al grows quicker than Si. Thus, the precipitated Si can become surrounded by Al, disrupting Si growth, so Si is the non-continuous phase, dispersed as flakes and needles (Fig. 2*b* and *c*).

When liquid Al–Si is cooled rapidly, the number of Si nuclei increases and the Si phase is refined; the effect of flake Si fracture is weakened, and the castings are consolidated. In practical die casting processes, the water cooling in the die sleeve and plunge tip produce sufficient cooling rates to give microstructures such as that in Fig. 2*a*.

In the centre of the biscuit, the cooling rate was smaller than at the periphery, but dendritic Si still occurred. Three possible causes have been identified. First, according to equation (10) and Fig. 8, the solidifying pressure decreased, which may lead to gas dissolved in the Al–Si coming out of solution, stirring the residual melt and

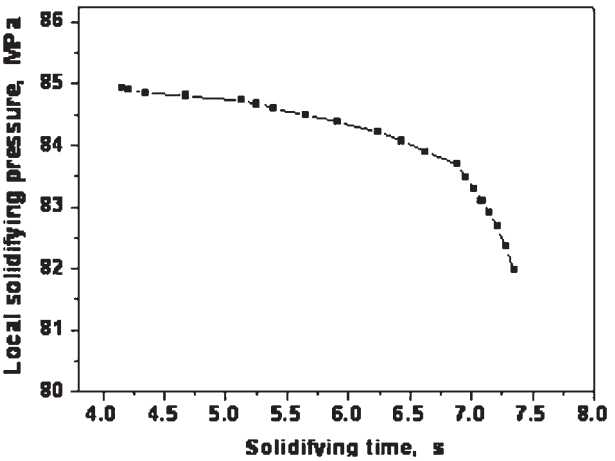

8 Local solidifying pressure changed with time

changing the solidification conditions. Second, nucleation on impurities precipitated from the melt (the specification for high pressure die casting alloys is less strict than that for conventional casting). Finally, nucleation on fragments separated from the solidified layer. The microstructure of the biscuit centre is like that shown in Fig. 2*d*, with the Si phase precipitated in spherical or granular form.

The outstanding character of die casting is high velocity and high pressure, the cavity was filled in 0·002–0·010 s and castings were produced at high pressure with high efficiency.[16] At high pressure, the melting point obeys the Clapyron equation

$$\frac{\mathrm{d}p}{\mathrm{d}T}=\frac{\Delta H_{\mathrm{m}}^{\mathrm{L}\to\mathrm{S}}}{T\Delta V^{\mathrm{L}\to\mathrm{S}}} \tag{11}$$

where $\Delta H_{\mathrm{m}}^{\mathrm{L}\to\mathrm{S}}$ is the enthalpy change and $\Delta V^{\mathrm{L}\to\mathrm{S}}$ is the volume change from liquid to solid. For Al–Si alloy, $\Delta H_{\mathrm{m}}^{\mathrm{L}\to\mathrm{S}}$ and $\Delta V^{\mathrm{L}\to\mathrm{S}}$ are positive, so the eutectic temperature increases with increasing pressure. Al–Si alloy eutectic points determined under different pressure are given in Table 4.[17]

Microhardness changed with Si morphologies. The average sizes of Si granules are 2·1 μm in Fig. 2*a* and 2.5 μm in Fig. 2*b* respectively. In Fig. 2*a*, the Si phase is distributed more evenly, so the value of microhardness was higher than that in Fig. 2*d*. In Fig. 2*b* and *c*, the Si arm spacings are 2 and 1 μm, and the arm thicknesses are 1·2 and 2 μm respectively, reflecting the higher microhardness for the structure in Fig. 2*b* than that in Fig. 2*c*.

No reports of compressive strength variation of Al–Si alloy at high temperature and high pressure were found in the literature. Instead, the Young's modulus variation with temperature given in Ref. 18 was used to estimate high temperature high pressure compressive strength and to calculate the local solidifying pressure. However, further research is required to acquire the strength at high temperature and high pressure. From Figs. 7 and 8 and equation (4), it can be concluded that the proportion of liquid metal solidified at <50 MPa was relatively small.

At large strain deformation, the yield strength σ can be expressed as[19]

$$\sigma=\sigma_0[1+\beta(\varepsilon+\varepsilon_{\mathrm{i}})]^{\mathrm{n}}\left[1+\frac{1}{G_0}\frac{\partial G}{\partial P}\frac{P}{\eta^{1/3}}+\frac{1}{G_0}\frac{\partial G}{\partial T}(T-300)\right] \tag{12}$$

where σ_0 is the initial value, β is a strain hardening coefficient, n is the strain hardening exponent, ε is the equivalent plastic, ε_{i} is the initial plastic strain, η is the compression ratio, G is the shear modulus and T is the temperature (K). The term

$$\frac{1}{G_0}\frac{\partial G}{\partial P}\frac{P}{\eta^{1/3}}$$

represents the effect of pressure hardening, and

$$\frac{1}{G_0}\frac{\partial G}{\partial T}(T-300)$$

represents the effect of thermal softening. Heat transfer coefficient between sleeve and Al–Si alloy is determined from temperature, pressure, density, latent heat of solidification and solidifying time. Heat transfer coefficient values from 1 to 170 kW m^{-2} $^{\circ}\mathrm{C}^{-1}$ have been reported,[17] and 20 kW m^{-2} $^{\circ}\mathrm{C}^{-1}$ was considered suitable to the present case.

In equation (7), solidified thickness is proportion to $t^{1/2}$. It can be seen from Fig. 7 that in the first 7 s solidification, equation (7) fits the data well; the values of α and β are −0·02005 and 0·77352 respectively. When the latent heat of solidification had been largely dissipated, solidification became much quicker and behaviour deviated from that predicted by equation (7). Equation (13a) may provide a better fit in the present case

$$t=0{\cdot}517938[(R-y)+1]^{0{\cdot}11816} \tag{13a}$$

or

$$(R-y)\propto t^{8{\cdot}4631} \tag{13b}$$

The microstructure in Fig. 2*b* was very different from that in Fig. 2*c*, and the composition of the Si phase was correspondingly different. As the melt cools, it would be inferred from equations (14)–(18)

$$\mathrm{Liquid}\to\mathrm{Al}+\mathrm{Si}\ (577^{\circ}\mathrm{C},\ 1\ \mathrm{atm}) \tag{14}$$

$$\mathrm{Liquid}\to\mathrm{Al}+\mathrm{Si}+\mathrm{Al_5FeSi}\ (575^{\circ}\mathrm{C},\ 1\ \mathrm{atm}) \tag{15}$$

$$\mathrm{Liquid}\to\mathrm{Al}+\mathrm{Si}+\mathrm{Al_{15}(Mn,Fe)_3Si_2}\ (573^{\circ}\mathrm{C},\ 1\ \mathrm{atm}) \tag{16}$$

$$\mathrm{Liquid}\to\mathrm{Al}+\mathrm{Si}+\mathrm{Mg_2Si}\ (555^{\circ}\mathrm{C},\ 1\ \mathrm{atm}) \tag{17}$$

$$\mathrm{Liquid}\to\mathrm{Al}+\mathrm{Si}+\mathrm{Al_2Cu}\ (525^{\circ}\mathrm{C},\ 1\ \mathrm{atm}) \tag{18}$$

that the Si phase precipitates from liquid successively as (Al + Si), (Al + Si + Al_5FeSi), (Al + Si + $Al_{15}(Mn,Fe)_3Si_2$), (Al + Si + Mg_2Si) and (Al + Si + Al_2Cu).[20]

However, pressure also influences the solute diffusion coefficients and hence the level of segregation. Equations (19) and (20) imply that solute diffusion coefficient diminishes markedly with increasing pressure[21,22]

$$D=\frac{RT}{\delta\eta_0}\exp\left[\frac{PV_0}{R(T+273{\cdot}15)}\right] \tag{19}$$

$$\frac{D}{D_0}=\exp\left[\frac{(1{\cdot}013\times10^5-P)V_0}{R(T+273{\cdot}15)}\right] \tag{20}$$

where R is the gas constant, T is the temperature of molten (°C), δ is the length of free journey for the atom, η_0 is the viscidity of a solution under usual pressure, P is the pressure, V_0 is the initial volume of liquid, D is the diffusing coefficient of solute under high pressure and D_0 is the diffusing coefficient under normal atmosphere.

From Fig. 8, the pressure at liquid/solid interface decreased markedly after 6·7 s solidification, solute can diffuse more easily and segregation would be more apparent. Defect bands were observed by Laukli *et al.*[23] and Gourlay *et al.*[24] when studying the effect of Si

Table 4 Eutectic temperature changed under pressure

Pressure, MPa	Al–Si alloy	Nominal point, %	Experimental point, %
69	…	12.6	16.5
100	Al–7Si, unmodified	12.6	15.4
100	Al–12Si, modified	12.6	18
150	…	12.6	18.7

content in hypoeutectic Al–Si high pressure die castings, and by Cao and Wessen[25] studying the microstructure of die cast AM50 magnesium components. These defect bands might be caused by segregation, besides other factors.

Summary and conclusions

Microstructure and microhardness of AlSi10Cu3 solidified in sleeve were studied; the differential equation of local solidifying pressure was deduced in horizontal cold chamber high pressure die casting, and the local solidifying pressure and temperature history were analysed in the expatiating of solidification conditions in this paper. Some conclusions on the base of present work can be summarised as follows.

The deduced differential equation of solidifying pressure explored that the local solidifying pressure was determined by two factors, the injecting force and the compressive strength of solidified alloy, and could explain why there existed porosity and pore in the last stage of solidification in high pressure die casting.

The local solidifying pressure changed with the thickness and strength of solidified layer, and in the last solidification, there existed porosity and pore because of the decreasing pressure. According to the deduced differential equation of liquid volume, the proportion of liquid metal solidified at pressure lower than 50 MPa was relatively small.

The microhardness relative to microstructure changed with locations, and the minimum value appeared in the position of $0{\cdot}4R$ from the biscuit centre. The morphologies of Si in the periphery and centre were in granules with different particle sizes, and in dendrite with different phase compositions in the other positions. The temperature distribution analysis carried with ANSYS in the present case showed that the solidified thickness was proportional to $t^{1/2}$ in the initial 7 s solidification and obeyed the equation $t=-0{\cdot}02005(R-y)^2+0{\cdot}77352(R-y)$. But in the last stage of solidification, the solidified layer thickened faster and revealed that they obeyed the equation $t=0{\cdot}517938[(R-\mathrm{y})+1)]^{0{\cdot}11816}$.

Acknowledgements

The authors would like to acknowledge the National Natural Science Foundation of China (Nos. 50375087 and 50301008), the Shandong Postdoctoral Innovation Special Fund (No. 200703073), the Project of Shandong Province Higher Educational Science and Technology Program (No. 50375087) and the Shandong Province Outstanding Research Award Fund for Young Scientists (No. 50375087) for financial support. The authors would also like to acknowledge the assistance of Q. H. Wang and G. L. Wei of the Jinan Huicheng Foundry Co. Ltd in sampling preparation. Discussion on die casting technology with Professor G. X. Sun and B. Y. Wu in Southeast University is gratefully acknowledged.

References

1. H. C. Liao, M. Zhang, Q. C. Wu, H. P. Wang and G. X. Sun: *Scr. Mater.*, 2007, **57**, 1121–1124.
2. S. W. Han, S. Kumai and A. Sato: *Mater. Sci. Eng. A*, 2001, **A308**, 225–232.
3. Q. Shi: 'Prediction of thermal distortion and thermal fatigue in shot sleeves', PhD thesis, Ohio State University, Columbus, OH, USA, 2002.
4. S. Birceanu: 'Improved design and durability of aluminum die casting horizontal shot sleeves', PhD thesis, Case Western Reserve University, Cleveland, OH, USA, 2005.
5. V. Joshi, A. Srivastava, R. Shivpuri and E. Rolinski: *Surf. Coat. Technol.*, 2003, **163–164**, 668–673.
6. B. Park: 'Effect of cavity pre-fill and geometry on flow patterns and air entrapment in the die cavity in cold chamber die casting', PhD thesis, Ohio State University, Columbus, OH, USA, 2001.
7. J. Zhou: 'Finite element analysis of flow and heat transfer of molten metal during the slow shot of die castings', PhD thesis, Carleton University, Ottawa, Ont., Canada, 2004.
8. R. Zamora, F. Faura, J. López and J. Hernández: *Int. J. Adv. Manuf. Technol.*, 2007, **33**, 266–276.
9. F. Faura, J. Lopez and J. Hernandez: *Int. J. Mach. Tools Manuf.*, 2001, **41**, 173–191
10. H. Y. Lu and W. B. Lee: *J. Mater. Process. Technol.*, 1999, **91**, 116–120.
11. R. Helenius, O. Lohne, L. Arnberg and H. I. Laukli: *Mater. Sci. Eng. A*, 2005, **A413–A414**, 52–55.
12. B. Zhang, D. M. Maijer and S. L. Cockcroft: *Mater. Sci. Eng. A*, 2007, **A464**, 295–305.
13. W. D. Griffiths, L. Xiao and D. G. McCartney: *Mater. Sci. Eng. A*, 1996, **A205**, 31–39.
14. E. W. Postek, R. W. Lewis, D. T. Gethin and R. S. Ransing: *J. Mater. Process. Technol.*, 2005, **159**, 338–346.
15. A. Yu, S. P. Wang, N. Y. Li and H. Hu: *J. Mater. Process. Technol.*, 2007, **191**, 247–250.
16. M. S. Dargusch, G. Dour, N. Schauer, C. M. Dinnis and G. Savage: *J. Mater. Process. Technol.*, 2006, **180**, 37–43.
17. Z.W. Chen: *Mater. Sci. Eng. A*, 2003, **A348**, 145–153.
18. S. P. Nikanorov, M. P. Volkov, V. N. Gurin, Y. A. Burenkov, L. I. Derkachenko, B. K. Kardashev, L. L. Regel and W. R. Wilcox: *Mater. Sci. Eng. A*, 2005, **A390**, 63–69.
19. T. J. Vogler and L. C. Chhabildas: *Int. J. Impact Eng.*, 2006, **33**, 812–825.
20. C. M. Chen, C. C. Yang and C. G. Chao: *Int. J. Cast Met. Res.*, 2004, **17**, 174–181.
21. Z. J. Wei, Z. L. Wang, H. W. Wang and L. Cao: *J. Mater. Sci.*, 2007, **42**, 7123–7128.
22. R. Xu: *Mater. Lett.*, 2005, **59**, 2818–2820.
23. H. I. Laukli, C. M. Gourlay, A. K. Dahle and O. Lohne: *Mater. Sci. Eng. A*, 2005, **A413–A414**, 92–97.
24. C. M. Gourlay, H. I. Laukli and A. K. Dahle: *Metall. Mater. Trans. A*, 2007, **38A**, 1833–1844.
25. H. Cao and M. Wessen: *Int. J. Cast Met. Res.*, 2005, **18**, 377–384.